http://informahealthcare.com/iht
ISSN: 0895-8378 (print), 1091-7691 (electronic)

Inhalation Toxicology

Inhal Toxicol, 2013; 25(4): 199–210
 DOI: 10.3109/08958378.2013.775197

informa healthcare

RESEARCH ARTICLE

Purification and sidewall functionalization of multiwalled carbon nanotubes and resulting bioactivity in two macrophage models

Raymond F. Hamilton Jr[1], Chengcheng Xiang[2,3], Ming Li[2], Ibrahima Ka[4], Feng Yang[3], Dongling Ma[4], Dale W. Porter[5], Nianqiang Wu[2], and Andrij Holian[1]

[1]Center for Environmental Health Sciences, University of Montana, Missoula, MT, USA, [2]Department of Mechanical and Aerospace Engineering, WVNano Initiative and [3]Department of Industrial and Management Systems Engineering, West Virginia University, Morgantown, WV, USA, [4]Institut National de la Recherche Scientifique, INRS-Énergie, Matériaux et Télécommunications, Boulevard Lionel-Boulet, Varennes, Québec, Canada, and [5]National Institute for Occupational Safety and Health, Morgantown, WV, USA

Abstract

This study examined the consequences of surface carboxylation of multiwalled carbon nanotubes (MWCNT) on bioactivity. Since commercial raw MWCNT contain impurities that may affect their bioactivity, HCl refluxing was exploited to purify raw ''as-received'' MWCNT by removing the amorphous carbon layer on the MWCNT surface and reducing the metal impurities (e.g. Ni). The removal of amorphous carbon layer was confirmed by Raman spectroscopy and thermogravimetric analysis. Furthermore, the HCl-purified MWCNT provided more available reaction sites, leading to enhanced sidewall functionalization. The sidewall of HCl-purified MWCNT was further functionalized with the –COOH moiety by HNO_3 oxidation. This process resulted in four distinct MWCNT: raw, purified, –COOH-terminated raw MWCNT, and –COOH-terminated purified MWCNT. Freshly isolated alveolar macrophages from C57Bl/6 mice were exposed to these nanomaterials to determine the effects of the surface chemistry on the bioactivity in terms of cell viability and inflammasome activation. Inflammasome activation was confirmed using inhibitors of cathepsin B and Caspase-1. Purification reduced the cell toxicity and inflammasome activation slightly compared to raw MWCNT. In contrast, functionalization of MWCNT with the –COOH group dramatically reduced the cytotoxicity and inflammasome activation. Similar results were seen using THP-1 cells supporting their potential use for high-throughput screening. This study demonstrated that the toxicity and bioactivity of MWCNT were diminished by removal of the Ni contamination and/or addition of –COOH groups to the sidewalls.

Keywords

Carboxylated, functionalized, inflammasome, MWCNT, toxicity

History

Received 27 November 2012
Revised 6 February 2013
Accepted 8 February 2013
Published online 13 March 2013

Introduction

Many properties of nanoparticles depend on their size and shape (Li et al., 2002; Tan et al., 2003; Zhang et al., 2010). Fiber-shaped (one-dimensional) nanoparticles exhibit different properties than round-shaped (zero-dimensional) nanospheres (Hamilton et al., 2009; Tafen et al., 2009; Wu et al., 2010; Zhi et al., 2011). One-dimensional carbon nanomaterials such as multiwalled carbon nanotubes (MWCNT) find extensive applications in structural and electronic devices due to their extraordinary thermal conductivity, mechanical properties, and electrical properties. Surface modification of MWCNT with functional moieties is a key step to extend their biological and industrial applications. Surface functional groups can alter the surface charge, functionality, and reactivity of the surface and enhance the stability and dispersibility of MWCNT. For example, functionalization of MWCNT with the –COOH moiety can change the wettability of MWCNT from hydrophobicity to hydrophilicity and provide active sites for further conjugation (Jain et al., 2011). However, ''as-received'' MWCNT from commercial vendors generally contain metal impurities (e.g. Ni) and a surface amorphous carbon layer. The presence of metal impurities and the surface amorphous carbon jeopardizes the intrinsic optical, electrical, and mechanical properties of MWCNT and can have undesirable biological activities. In addition, the surface amorphous layer causes interference with the functionalization on the sidewall of MWCNT (Wang et al., 2009). Therefore, it is necessary to remove amorphous impurities and residual metals in order to functionalize the genuine sidewall of MWCNT.

Owing to the unique physical and chemical characteristics, MWCNT may have distinctive biological effects (Porter et al., 2010; Wang et al., 2010). In particular, MWCNT contaminants, particularly Ni, resulting from the production process have been implicated in the cytotoxicity and bioactivity of single-walled carbon nanotubes (Liu et al., 2007) and have been shown to contribute to the bioactivity of MWCNT

Address for correspondence: Andrij Holina, Center for Environmental Health Sciences, University of Montana, Missoula, MT 59812, USA. Tel: +1 (406) 243-4018. Fax: +1 (406) 243-2807. E-mail: andrij.holian@umontana.edu

(Hamilton et al., 2012a,b). Carboxylation of MWCNT can result in a less hydrophobic, more negatively charged particle, which could affect the mechanism(s) of how cells bind and internalize MWCNT, and consequently affect bioactivity. For example, studies have demonstrated that many negatively charged micron-sized particles are taken up by phagocytic cells such as macrophages using scavenger receptors (Hamilton et al., 2006; Jozefowski et al., 2006), while the mechanisms of uptake of neutral and positively charged particles are less clear.

Several studies have linked phago-lysosomal permeablization accompanied by cathepsin B release, which initiates NLRP3 inflammasome assembly, and Caspase-1 activation (Arend et al., 2008; Martinon et al., 2009; Tschopp & Schroder, 2010). While other more recent studies have suggested that toxic nanomaterials can initiate this lysosomal damage leading to NLRP3 inflammasome activation, the exact mechanisms are unkown at this time (Palomaki et al., 2011; Yazdi et al., 2010). The endpoints in this study, toxicity, NLRP3 inflammasome activation, particle uptake, and Caspase-1 activation, are designed to explore the mechanisms with a set of four MWCNT that vary with regards to surface properties by a series of modifications.

The hypothesis in this study is that these surface modifications, in particular, the addition of carboxyl groups to MWCNT will reduce or eliminate the bioactivity of the nanomaterials in macrophages exposed *in vitro*. The removal of surface amorphous carbon and residual metals in MWCNT was approached through hydrochloride (HCl) refluxing treatment. MWCNT were functionalized with the –COOH moiety via nitric acid oxidation. Studies of the bioactivity of the MWCNT were conducted using primary alveolar macrophages (AM) isolated from C57Bl/6 mice and compared to differentiated THP-1 cells with respect to toxicity and activation of the NLRP3 inflammasome.

Materials and methods

Purification of MWCNT

Typically, 300 mg of ''as-received'' MWCNT from a commercial source (Stock#: 1231YJ; Nanostructured & Amorphous Materials, Inc., Houston, TX) were added to a 250-ml three-neck flask containing 100 ml of hydrochloride (con. 36.5%) and then sonicated for 30 min. After being refluxed at 80–90 °C for 4 h, the suspension was naturally cooled down to room temperature and subsequently centrifuged. The resulting supernatant was removed by decantation. Black precipitates were washed using deionized water and ethanol, followed by successive centrifugation and decantation until the pH value reached to 6.0–7.0. The resulting powders were dried in a vacuum oven at room temperature overnight and then stored in a vial for use.

Functionalization of MWCNT

Carboxylated MWCNT (COOH–MWCNT) were prepared by refluxing the MWCNT in HNO_3 (con. 63%). Typically, 300 mg MWCNT were added to a three-neck flask containing 100 ml of HNO_3, followed by refluxing at about 110 °C for 12 h. The black solution was then centrifuged and washed with deionized water to remove HNO_3 until the solution was neutral. The resulting powders were dried at room temperature in a vacuum oven for at least 24 h.

Characterization of MWCNT

The Ni content was measured by inductively-coupled plasma mass spectrometry (ICP-MS; Santa Fe Springs, Exova, CA). The MWCNT were observed under a JSM-7600F field emission scanning electron microscope (SEM; JEOL Ltd., Tokyo, Japan) and a JEM 2100 high-resolution transmission electron microscope (HRTEM; JEOL Ltd) at an operation voltage of 200 kV. The ultraviolet–visible (UV–vis) absorption spectra were collected in the range of 200–800 nm with a Shimadzu UV-2550 instrument (Shimadzu Co., Kyoto, Japan). Fourier-transform infrared (FTIR) spectra were obtained under the transmission mode with Thermo Nicolet 6700 spectrometer (Thermo Nicolet, Madison, WI). Raman spectra were collected using a Renishaw inVia Raman spectrometer (Renishaw PLC, Gloucestershire, UK) equipped with the 514.5 nm line of Ar^+ ion laser as the excitation source. Thermogravimetric analysis (TGA) was carried out with TGA Q500 (TA Instruments, New Castle, DE) from 50 °C to 1000 °C at a heating rate of 10 °C/min under a nitrogen flow at 60 ml/min. The MWCNT were characterized with X-ray photoelectron spectroscopy (XPS) with PHI 5000 Versa Probe system (ULVAC-PHI, Inc., Chigasaki, Japan). The XPS spectra were calibrated with the reference to the C 1s peak of aliphatic carbon at 284.8 eV. Fitting of XPS spectra was performed using PHI Multipak™ software with the Gauss-Lorentz line and Shirley background subtraction. The surface charge of the MWCNT was measured using the zeta potential mode of the Malvern Zetasizer Nano ZS (Malvern Instruments Ltd., Worcestershire, UK). The ''as-received'', purified, and functionalized MWCNT were dispersed into deionized water by ultrasonication to achieve a suspension of 10 mg/l. Ten measurements were conducted for all samples, and the average values were reported to present the results of surface charge.

Experimental procedures

Animals

C57Bl/6 (2 months old, male) were housed in controlled environmental conditions (22 ± 2 °C; 30–40% humidity, 12-h light:12-h dark cycle) and provided food and water *ad libitum*. All procedures were performed under protocols approved by the IACUC of the University of Montana.

MWCNT suspensions

All nanotubes were weighed and suspended in phosphate-buffered saline (PBS)/7.5% bovine serum albumin (BSA) solution (A8412; Sigma-Aldrich, St. Louis, MO) as described elsewhere (Buford et al., 2007). Nanotube suspensions were sonicated for 1 min in a Masonix cup-horn sonicator (XL2020; Misonix, Farmingdale, NY) attached to a Forma circulating water bath at 550 W and 20 Hz at a stock concentration of 5 mg/ml.

AM isolation

Mice were euthanized by sodium pentobarbital (Euthasol™), and the lungs with the heart were removed. Lung lavage was performed using ice-cold PBS (pH 7.4). Lung lavage cells were isolated by centrifugation (400×*g*, 5 min, 4 °C), and cell counts were obtained using a Coulter Z2 particle counter (Beckman Coulter, Miami, FL).

Cell culture

The AM cells were suspended in RPMI media supplemented with 10% fetal bovine serum, 0.05 mM 2-mercaptoethanol, sodium pyruvate, and supplemented with an antimycotic/antibiotic cocktail (Mediatech, Manassas, VA). Cells were suspended at 1×10^6 cells per ml and then lipopolysaccharide (LPS; Sigma) at 20 ng/ml was added to stimulate pro-interleukin-1β (pro-IL-1β) and pro-IL-18 formation. A 100 µl sample (100 000 cells) of cells were exposed to each MWCNT (ex: high-dose 100 µg/ml equivalent to 10 µg/10^5 cells equivalent to 31.25 µg/cm^2 (10 µg on 0.32 cm^2)) and experiments were conducted in 96-well plates for 24 h in 37 °C water-jacketed CO_2 incubators (ThermoForma, Houston, TX). Particle concentrations ranged from 0, 10, 25, 50, and 100 µg/ml. One experiment used a cathpsin B inhibitor (CA-074-Me; Peptides International, Louisville, KY) at 10 µM or a Caspase-1 inhibitor (Ac-Try-Val-Ala-Asp-CMK; AnaSpec, Fremont, CA) at 20 µM, which were preincubated with the AM for 30 min prior to particle exposure at 50 µg/ml or 15.6 µg/cm^2 for 24 h. Media was collected for IL-1β assay, and the cell viability was determined by MTS assay. Imaging experiments were conducted without the LPS co-culture for shorter time points (1, 2 and 4 h).

Toxicity assay

Cell viability was determined by MTS reagent using the CellTiter^{96} assay (Promega, Madison, WI) according to the manufacturer's protocol. This assay used a colorimetric dye read by a colorimetric plate reader (Molecular Devices, Sunnyvale, CA). In order to avoid artifacts in the optical density values, steps were taken to remove the MTS reagent (transferring it into another plate) from the cell/particle mixture adhered to the plate bottom. The formation of bubbles was avoided and the plate was read at 490 nm.

Cytokine assays

Mouse and human IL-1β DuoSets were obtained from R&D Systems (Minneapolis, MN), and enzyme-linked immunosorbent assay (ELISA) was performed according to the manufacturer's protocol. Antibodies for mouse and human IL-18 ELISA were obtained from R&D Systems and performed as previously described (Hamilton et al., 2009). Plates were read at 450 nm.

Electron microscopy

Isolated AM from C57Bl/6 mice were exposed to MWCNT at 50 µg/ml for 1 h in suspension culture. The cells were washed once in PBS and resulting macrophage suspensions were fixed in 2.5% EM grade glutaraldehyde in cacodylate buffer at pH 7.2 (Electron Microscopy Sciences (EMS), Hatfield, PA). The cells were then rinsed in distilled water (dH_2O) and resuspended in 1% osmium tetroxide (EMS) for 1 h and rinsed in dH_2O. The cells were dried in a graded ethanol series followed by embedding of the cell pellet in epoxy resin. Thin sections were stained with 2% uranyl acetate (EMS) for 30 min at room temperature, rinsed in dH_2O, and stained for 5 min with Reynolds lead citrate stain (EMS). The cells were imaged in a Hitachi H-7100 transmission electron microscope (Chula Vista, CA) at 75 kV.

Fluorescence microscopy

Fluorescent confocal photomicrographs of lysosomes were obtained in C57Bl/6 AM cells stained with acridine orange (KP31322; 1:1000 Calbiochem (EMD Biosciences, La Jolla, CA)) ± MWCNT (50 µg/ml) for 2 h and 4 h in culture on 96-well glass-bottom plates (# 0; MatTek Corp, Ashland, MA). Images were made with an Olympus Fluoview 1000 laser scanning confocal mounted on an inverted IX81microscope with laser excitation (Center Valley, PA). The processing software was Olympus FV, Version 2.1b (Olympus America Inc., Center Valley, PA). The acridine orange filter uses 488 nm excitation and a 525-nm emission wavelength. All images were at 600×, using a 60× oil objective.

Caspase-1 imaging and quantitation

Isolated macrophages were counted and mixed with MWCNT (50 µg/ml) in RPMI media and plated in eight-well chambered cover slips (Lab-Tek; Fisher Scientific, Houston, TX). This was incubated for 2 h at 37 °C and FAM FLICA fluorescent Caspase-1 substrate was added at 2× recommended concentration (Immunochemistry Technologies, Bloomington, MN). This was incubated for an additional hour. The wells were washed with PBS twice and HSC blue nuclear mask (Molecular Probes, Eugene, OR) was added in phenol-free RPMI media (Sigma) at 1:2000. This was incubated at 37 °C for an additional 10 min before analysis using a CompuCyte iCys cytometer (Westwood, MA). The Caspase-1 signal was detected using a 20 W 488 nm laser as the excitation source and a PMT detector with a 530/30 nm bandpass filter in front. The nuclear staining was exited with a 50 W 405 nm laser and detected with a 440/30 nm bandpass filter/PMT detector set. The iCys was programmed to make 0.25 µm x-steps on an automated stage using a 40× inverted objective to interrogate 49.5 mm^2 each step. Regions were defined in each well to include an adequate number of cells and a scan performed. Individual passes of the 488 nm and 40 nm lasers were used to avoid any spectral overlap of the two fluorescent signals. A threshold of ''blue'' fluorescence was set such that the software draws a contour around the nucleus of the cell. The contour was then expanded by 22 pixels to include the cytoplasm of the cell. The total relative ''green'' fluorescence (pixel by pixel) within the integrated contour was then measured and sent as electronic pulses to the computer, which converts them to digital signals. Each cell (as defined by nuclear staining) was plotted on a histogram showing Green Mean Fluorescent Intensity (MFI), which is the per cell integral (total fluorescence/cell). An average of 1500 cells were interrogated to get statistical significance. In

the instance of active Caspase-1, a clear ''positive'' peak emerged and a marker to show percentage of positive events was drawn, in addition to reporting the overall shift of MFI.

Human THP-1 cell line culturing

Human monocytic cell line THP-1 (obtained from ATCC, Manassas, VA) were cultured at low passage in the same media described above and under the same conditions (cell numbers, particle exposures, assays, etc . . .), with the exception that the cells were differentiated 24 h prior to MWCNT particle exposure by the addition of 82 nM phobol 12-myristate 13-acetate (PMA; Sigma) as described elsewhere (Hamilton et al., 2012b). The resulting transformed adherent cells were scraped and washed in PBS (Sigma), centrifuged at $400\times g$, and counted as described above. The MWCNT exposure conditions were identical to those described above.

Statistical analyses

Statistical analyses involved comparison of means using a two-way ANOVA followed by Bonferroni's test to compensate for increased type I error. Two-tailed statistical significance is a probability of type I error at less than 5% ($p < 0.05$). Statistical power was greater than 0.8. The minimum number of experimental replications was 3. Graphics and analyses were performed on PRISM 5.0 (Graphpad, La Jolla, CA).

Results

Microstructure and surface chemistry of MWCNT

HCl refluxing was adopted to remove amorphous carbon and the residual Ni catalyst as shown in the scheme in Figure 1. It is known that a large number of defects exist on the surface of amorphous carbon, which facilitates relatively easy adsorption of hydroxyl groups onto it during HCl reflux treatment (Datsyuk et al., 2008). On the other hand, residual metal catalysts can react with HCl to form metal chloride. HCl is a nonoxidative acid and cannot introduce oxygen-containing groups, but it can enhance the exposure of amorphous carbon encapsulated in graphitic carbon (Datsyuk et al., 2008). Therefore, the hydroxyl group can be grafted onto the disordered carbon, leading to increased water dispersibility. Hydroxylated amorphous carbon and nickel chloride will remain in the liquid phase, while the MWCNT deposit. Based on the above analysis, hydroxylated amorphous carbon and metal chloride are easily separated from MWCNT by centrifugation and decantation procedures.

HNO_3 oxidation is a common approach that imparts the –COOH functional group onto MWCNT because of its simplicity and efficiency (Brozena et al., 2010; Feng et al., 2005; Forrest & Alexander, 2007; Pumera, 2007; Worsley et al., 2009). In light of this, HNO_3 oxidation was used to investigate the effect of HCl treatment on the functionalization of MWCNT. As shown in the Supplemental Section Figure S1(a), ''raw'' and HCl-purified MWCNT have poor water solubility. In contrast, after HNO_3 oxidation, both carboxylated forms of MWCNT showed very good water solubility and suspensions are stable for up to two months. The zeta potential of the purified MWCNT was measured to be −9.76 mV while the –COOH-functionalized one was −13.8 mV. The reason was that the –COOH moiety can be dissociated into negative charge $–COO^-$ due to the low isoelectric point, leading to more negative surface charge. Supplemental Figure S1(b) shows the UV–vis absorption spectra of all the MWCNT samples. Both the ''raw'' MWCNT and HCl-treated samples have characteristics of van Hove singularities that reflect their unique electronic properties (Hudson et al., 2004; Long et al., 2008; Peng et al., 2003; Wang et al., 2006; Zimmerman et al., 2000). However, HNO_3 oxidation treatment produced much smoother optical absorption curves because of the disappearance of van Hove singularities and enhanced water solubility (Brozena et al., 2010; Datsyuk et al., 2008; Feng et al., 2005).

It can be seen from the SEM images in Figure 2 that either the HCl treatment or HNO_3 oxidation caused no observable structure damage to MWCNT, which is essential to maintain the tubular morphology of MWCNT. Any structural change will affect the mechanical strength as well as electric and optical performances. However, the TEM images (insets) reveal that the MWCNT exhibited much clearer tubular structure after HCl purification.

Metallic Ni, which functions as a catalyst during MWCNT production, generally is the main residual metal in ''raw'' MWCNT (Worsley et al., 2009). HCl reflux treatment is capable of partially removing it, which has been confirmed by the ICP-MS measurement. The ''raw'' MWCNT contain 2.2 wt% Ni and 0.08 wt% iron (Fe). After HCl treatment, the Ni content was reduced by 0.96 wt%, and iron was not detected by ICP-MS. After nitric acid (HNO_3) treatment, 0.07% wt% Ni was detected. TGA was performed to investigate the thermal stability of ''raw'' and purified MWCNT (Supplemental Figure S2a). NH_4OH/H_2O_2 treatment, which was reported to be an efficient approach for the removal of amorphous carbon on MWCNT was used as the control experiment (Datsyuk et al., 2008). The onset temperature of

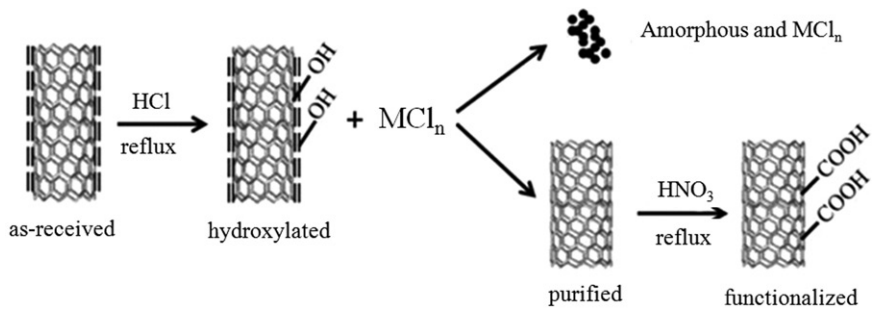

Figure 1. Schematic illustration of MWCNT purification and sidewall functionalization.

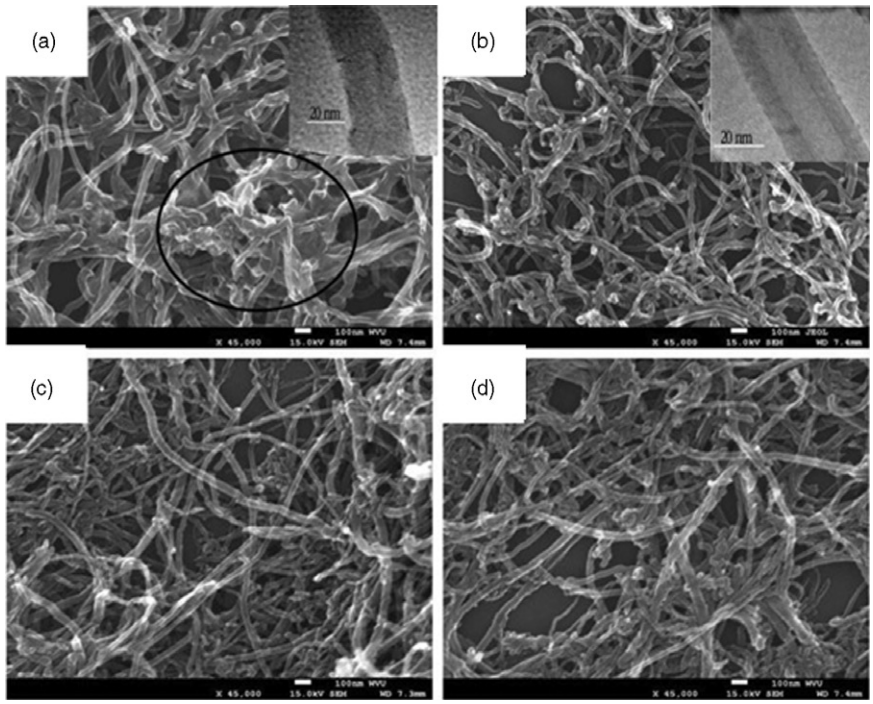

Figure 2. SEM images of (a) ''as-received'' MWCNT, (b) HCl-purified MWCNT, (c) HNO_3-treated MWCNT and (d) HCl/HNO_3-treated MWCNT. Insets are TEM images of the corresponding MWCNT; scale bar: 20 nm.

thermal loss for the ''raw'' MWCNT was 660 °C, which was ascribed to the thermal oxidation of the amorphous carbon. The HCl-treated MWCNT showed the thermal loss above 760 °C showing higher thermal stability than the NH_4OH/H_2O_2-treated and the ''raw'' MWCNT. This indicates that the HCl treatment removed the surface amorphous carbon effectively. To prove this point, Raman spectra were taken of the MWCNT (Supplemental Figure S2b). Each of Raman spectra consists of the D band and the G band positioned at 1346 cm^{-1} and 1571 cm^{-1}, respectively. The D band is attributed to the disordered species such as amorphous carbon and the lattice defects, while the G band is ascribed to the skeletal stretching vibration mode of the graphitic component (SP^2 bonding) (Ferrari et al., 2006). Hence the I_D/I_G ratio (peak intensity ratio) reflects the content of amorphous carbon and the defects in the honeycomb lattice. The I_D/I_G ratio was reduced after the HCl treatment, which reflects the reduced amount of surface amorphous carbon in comparison with the ''raw'' MWCNT. Nevertheless, HNO_3 oxidation increased the I_D/I_G ratio, which was due to grafting of the –COOH functional groups to the surface of MWCNT. The sample that was subject to HCl treatment plus HNO_3 oxidation had the highest I_D/I_G ratio among all the four types of samples, which indicated that more –COOH groups were present in this sample. This suggests that the HCl treatment enhanced the sidewall functionalization with the –COOH groups. This point was further supported by FTIR and XPS results below.

Figure 3 shows the FTIR spectra obtained from ''raw'', HCl-treated, HNO_3-treated, and HCl/HNO_3-treated MWCNT. Both the ''raw'' and the HCl-treated MWCNT showed skeletal vibration of aromatic rings around 1640 cm^{-1} and 1566 cm^{-1} (Peng et al., 2003). In addition, the peaks at 1384 cm^{-1}, 1030 cm^{-1}, and 1200 cm^{-1} are ascribed to the symmetric C–H deformation vibration, the C–O stretching vibration, and the C–C deformation vibration, respectively

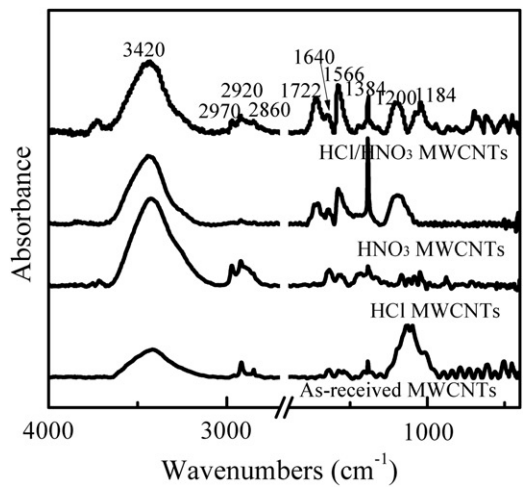

Figure 3. FTIR spectra of ''as-received'' MWCNT, HCl-purified MWCNT, HNO_3-treated MWCNT, and HCl/HNO_3-treated MWCNT.

(Shao et al., 2007). After HNO_3 oxidation, the C=O stretching vibration appeared at 1722 cm^{-1} (Lim et al., 2007; Ramanathan et al., 2005; Wu et al., 2004). Furthermore, the intensity ratio of the 1722 cm^{-1} peak to the 1566 cm^{-1} peak was considerably higher in the HCl/HNO_3-treated sample than that in the HNO_3-treated MWCNT, which suggests that HCl refluxing enhanced the sidewall functionalization with the –COOH groups.

The XPS is a powerful tool to quantify the elemental content and to identify the chemical structure. The four types of MWCNT exhibited the difference in the XPS spectrum of the C 1s core level (Figure 4). The deconvoluted components of the C 1s peaks at 284.8 eV, 286.2 eV, and 288.5 eV correspond to the –C–C, –C–OH, and –C=O bonds, respectively (Ramanathan et al., 2005). Only two components related to the –C–C and –C–OH bonds were present in both the ''raw'' and the HCl-treated MWCNT. In contrast, after HNO_3

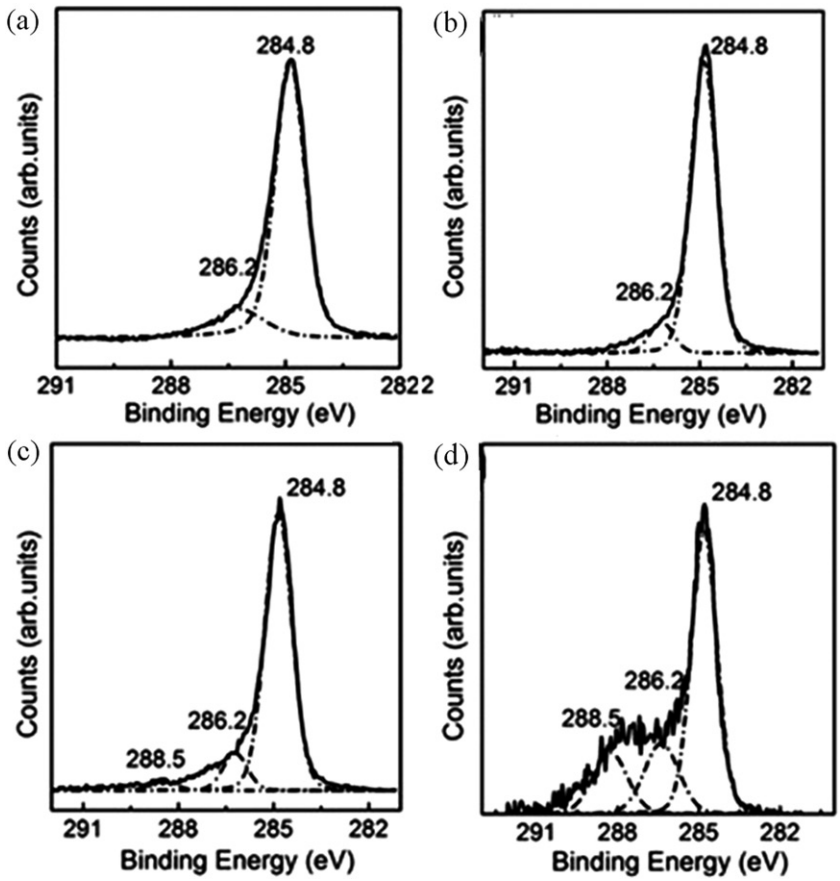

Figure 4. XPS spectra of the C 1s core level (a) ''as-received'' MWCNT, (b) HCl-treated MWCNT, (c) HNO_3-treated MWCNT and (d) HCl/HNO_3-treated MWCNT.

oxidation of the ''raw'' MWCNT, the –C=O peak at 288.5 eV was clearly observed. Moreover, the HCl/HNO_3-treated MWCNT showed an enhanced –C=O peak, which demonstrates that more –COOH groups were grafted onto the surface of the MWCNT after HCl refluxing. Therefore, the Raman, FTIR, and XPS data were consistent with each other, which strongly supports that the HCl treatment enhanced sidewall functionalization due to the removal of surface amorphous carbon. The above experimental results show that the nonoxidative HCl reflux can facilitate the functionalization of MWCNT by removing surface amorphous carbon.

Relative toxicity and bioactivity of modified MWCNT

The four MWCNT were tested to assess toxicity and potential to activate the NLRP3 inflammasome using freshly isolated primary C57Bl/6 AM. The toxicity results shown in Figure 5(a) demonstrate that the functionalized MWCNT were relatively nontoxic compared to the raw or purified MWCNT at high particle concentrations (50 μg/ml or greater). Purification had no apparent effect on toxicity. The results in Figure 5(b,c) show concentration-dependent inflammasome activation demonstrated by particle-exposed AM releasing IL-1β and IL-18, respectively. In this assay (IL-1β and IL-18), raw MWCNT produced the largest response followed by the purified MWCNT, which was significantly lower than the raw MWCNT at 25 and 50 μg/ml. Both forms of functionalized MWCNT elicited a significantly muted response compared to either the raw or purified MWCNT.

Blocking of inflammasome activity by Caspase-1 and cathepsin B inhibitors

To clearly demonstrate the role of phago-lysosomal disruption and NLRP3 inflammasome activation from the MWCNT, all four MWCNT at 50 μg/ml, were cultured with and without cathepsin B inhibitor CA-074-Me (10 μM) or the Caspase-1 inhibitor Ac-Try-Val-Ala-Asp-CMK (20 μM), respectively, and 50 μg/ml MWCNT for 24 h (Figure 6). Figure 6(a) demonstrates that the inhibitors are not effective in reversing the toxicity of the raw or pure MWCNT. However, the cathepsin B and Caspase-1 inhibitors significantly reduced IL-1β release from both MWCNT exposures (Figure 6b). The cathepsin B inhibitor was slightly more effective, completely eliminating the IL-1β release. These data also clearly demonstrate that cytotoxicity and infammasome activation are unrelated processes with regard to MWCNT AM exposure, eliminating the possibility of inflammasome-mediated apoptosis or pyroptosis as a confounding interpretation of the AM response.

Macrophage uptake of MWCNT

To demonstrate that the difference in toxicity and inflammasome activation were not due to differential uptake of particles, EM images of AM following 1 h of MWCNT exposure were examined (Figure 7A–F). This examination revealed that all particles regardless of modification were taken up by the AM. However, there was a difference in how the particles were processed within the cells. The purified MWCNT were taken up in large vacuoles or phago-lysosomes

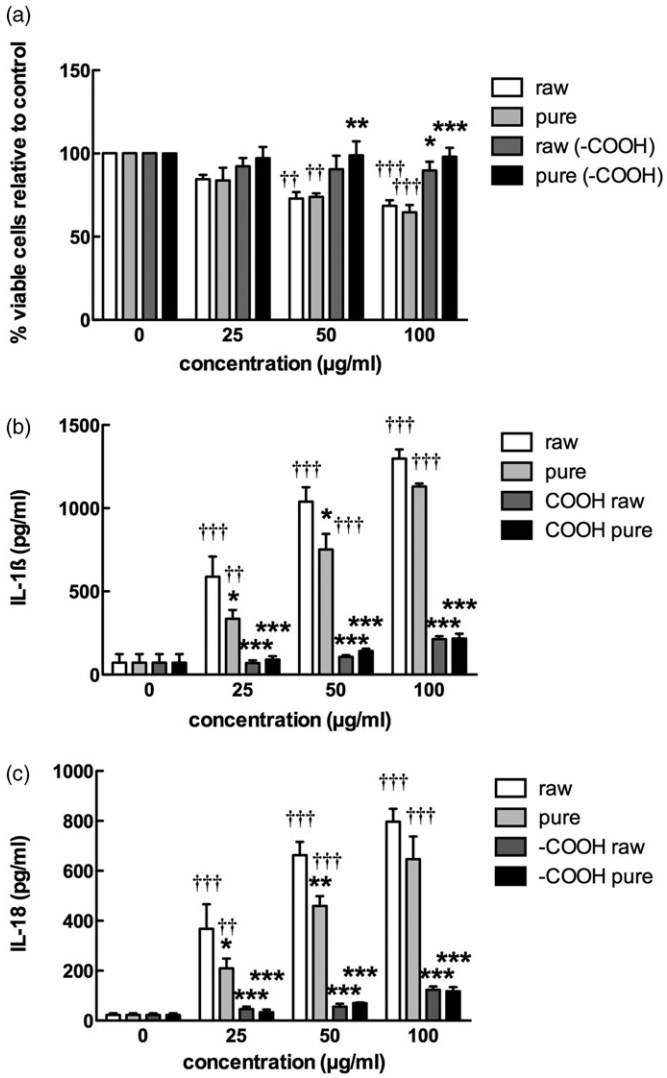

Figure 5. Bioactivity of the four MWCNT in the C57Bl/6 alveolar macrophage model. Cells were exposed to 25, 50, or 100 µg/ml of each MWCNT for 24 h with LPS co-culture (20 ng/ml), and the following endpoints were evaluated: (a) cell viability by MTS assay expressed as mean ± SEM percent relative to unstimulated control cultures, (b) IL-1β production expressed as mean ± SEM, (c) IL-18 production expressed as mean ± SEM. Asterisks indicate $*p<0.05$, $**p<0.01$, or $***p<0.001$ by Bonferroni's correction following two-way ANOVA compared to ''raw'' at each corresponding concentration. Daggers (†) indicate comparison to the 0 µg/ml or baseline condition, with the number indicating the significance level similar to the asterisks. Sample $n=3$.

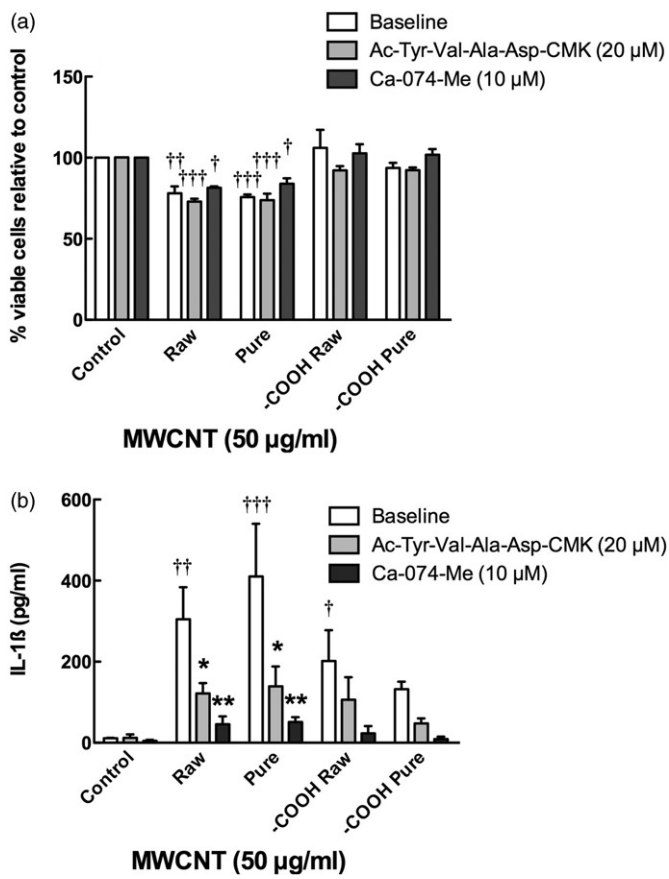

Figure 6. Blocking inflammasome activation by cathepsin B and Caspase-1 inhibitors. Cells were preincubated with either cathepsin B inhibitor (Ca-074-Me at 10 µM) or Caspase-1 inhibitor (Ac-Try-Val-Ala-Asp-CMK at 20 µM) for 30 min prior to particle exposure at 50 µg/ml for 24 h, and the following endpoints were evaluated: (a) cell viability by MTS assay expressed as mean ± SEM percent relative to unstimulated control cultures, (b) IL-1β production expressed as mean ± SEM. Asterisks indicate $*p<0.05$ or $**p<0.01$ by Bonferroni's correction following two-way ANOVA compared to no inhibitor condition for each corresponding particle. Daggers (†) indicate comparison to the control or baseline condition, with the number indicating the significance level similar to the asterisks. Sample $n=3$.

(Figure 7B,C; higher magnification) and did not appear to be in the cytoplasm. In contrast, the two functionalized MWCNT appeared not to be in large vacuoles but rather were more evenly distributed throughout the cytoplasm in smaller phago-lysosomal structures or absent organization structure (Figure 7D–F; higher magnification).

Lysosomal disruption in macrophages exposed to raw or purified MWCNT

Since phago-lysosomal rupture, disruption, or possible malformation is an initial step in the inflammasome activation process from particle exposure (Cassel et al., 2009; Drenth & van der Meer, 2006; Martinon et al., 2009; Tschopp & Schroder, 2010), AM were stained with acridine orange to label lysosomes in cells exposed to the purified and functionalized MWCNT for 2 and 4 h. The results shown in Figure 8(b,e) demonstrated that phago-lysosomal damage, indicated by the lack of punctate staining, was apparent in AM exposed to purified MWCNT at both 2 and 4 h post-exposure times. In contrast, AM exposed to functionalized MWCNT showed discrete punctate staining consistent with intact phago-lysosome formation (Figure 8c,f) at both observation times, respectively. The macrophage response to the raw MWCNT and functionalized raw MWCNT particles was exactly the same as the corresponding purified MWCNT and functionalized purified MWCNT particles (data not shown).

Caspase-1 induction in macrophages

Additional evidence of phago-lysosomal disruption leading to NLRP3 assembly was supplied by staining AM exposed to MWCNT for a down-stream event (Caspase-1 induction) by a fluorescent substrate as described in Methods. Figure 9 shows computer-generated images of relative Caspase-1 intensity within AM exposed to the various MWCNT (green color with gated signal in insets). The raw MWCNT-exposed cells

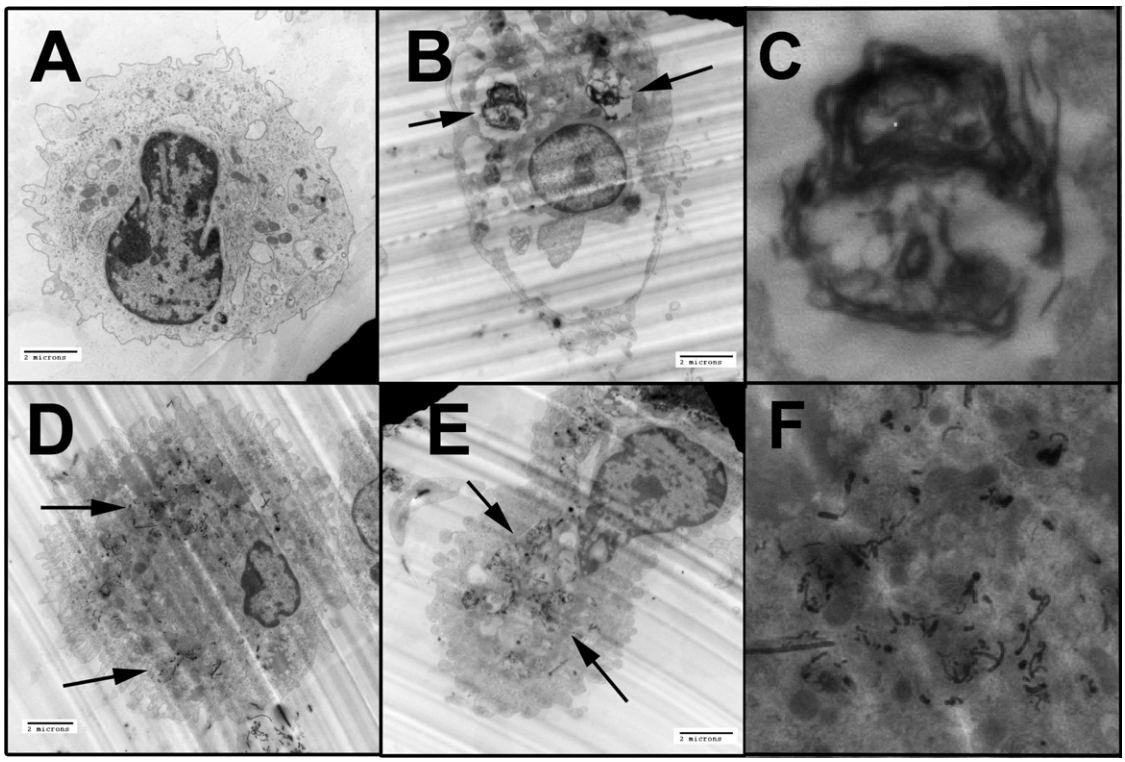

Figure 7. Representative TEM photomicrographs of C57BL/6 alveolor macrophages taking up MWCNT after 1 h of exposure in culture without the presence of LPS. Black arrows indicate areas of particle uptake. (A) Unstimulated control macrophage. (B) Macrophage taking up purified MWCNT, note the descrete lysosome/vacuole formation around the carbon material. (C) Magnified inset from Figure 7(B) (left arrow) of MWCNT encapsulated in a discrete lysosome. (D) Macrophage taking up –COOH functionalized raw ''as-produced'' MWCNT. The material is more dispersed within the cytoplasm. (E) Macrophage taking up –COOH functionalized, purified MWCNT. (F) Magnified inset from Figure 7(D) (upper left arrow) of funtionalized, raw MWCNT within the alveolar macrophage. The material distributes within the cytoplasm in the absence of lysosomal formation. All images taken at 7000×, except for (C) and (F).

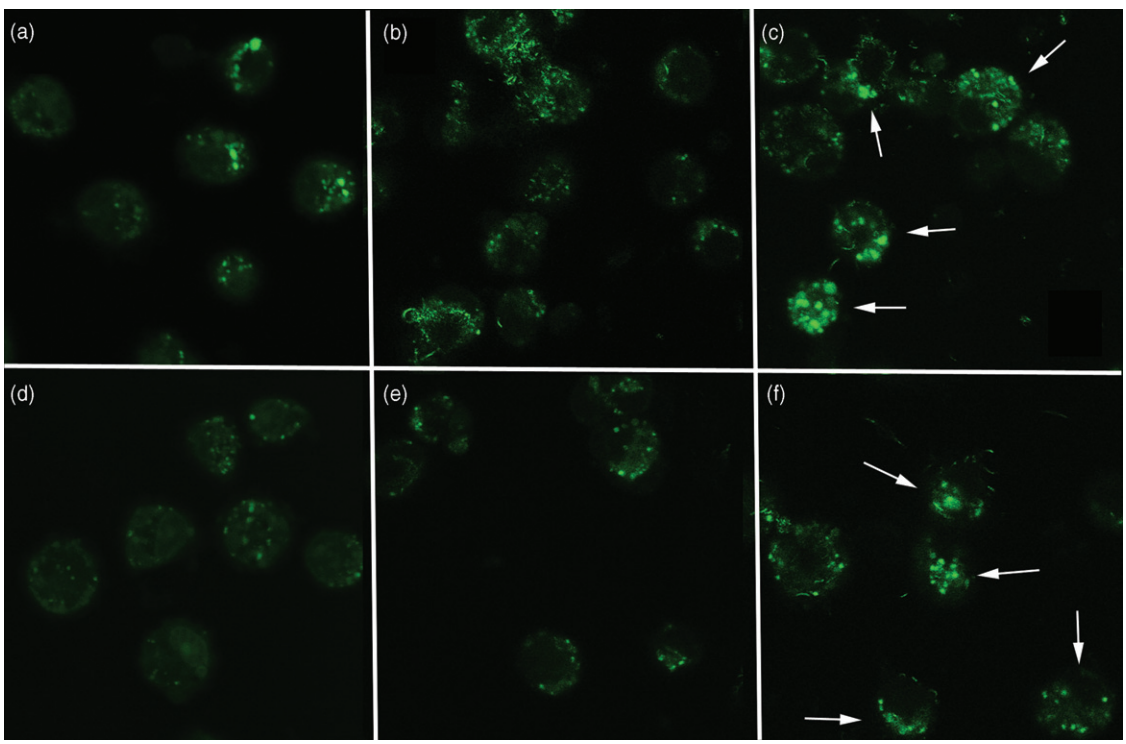

Figure 8. Representative fluorescent photomicrographs of C57BL/6 alveolor macrophages taking up MWCNT after 2 and 4 h of exposure in culture, without the presence of LPS, stained with acridine orange to detect lysosome formation. White arrows indicate cells with lysosomal stability following MWCNT exposure. (a) No particle control macrophages at 2 h. (b) Macrophages taking up purified MWCNT at 2 h post-exposure. (c) Macrophages taking up –COOH functionalized purified MWCNT at 2 h post-exposure. (d) No particle control macrophages at 4 h. (e) Macrophages taking up purified MWCNT at 4 h post-exposure. (f) Macrophages taking up –COOH functionalized purified MWCNT at 4 h post-exposure. The lack of punctate green staining in (b) and (e) indicate possible lysosomal damage, malformation, and/or leakage. All images taken at ×600 oil.

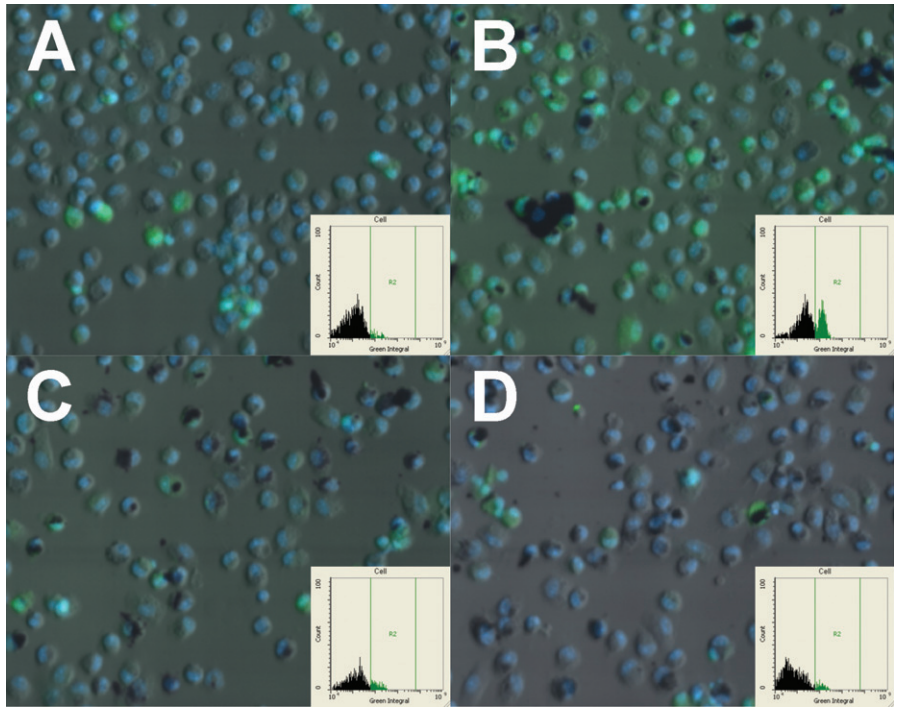

Figure 9. Computer generated (iCys) images of C57BL/6 alveolar macrophages exposed to FAM FLICA green Caspase-1 substrate. (A) No-particle control cells at 3 h. (B) Cells exposed to raw MWCNT for 3 h. (C) Cells exposed to functionalized raw MWCNT for 3 h. (D) Cells exposed to functionalized pure MWCNT for 3 h. Green fluorescence indicates Caspase-1 signal. Blue fluorescence is the nucleus. Insets show gated positive signal for Caspase-1 (only present in panel B).

(Figure 9B) showed a substantial increase in Caspase-1 staining compared to control cells (Figure 9A). This was not apparent in either of the functionalized MWCNT-exposed cells after 3 h (Figure 9C,D). The pure MWCNT-exposed cells showed a similar but slightly reduced Caspase-1 signal (data not shown). These images also show how the AM take up more of the functionalized MWCNT regardless of purity or how much of the suspended material actually gets to the cell. This also serves to further suggest that functionalized and raw MWCNT are taken up by different mechanisms depending on the surface state of the particles.

Human transformed THP-1 cell confirm the response model to MWCNT

The above studies were performed using primary murine AM (Figures 5–9). In order to evaluate whether similar results could be obtained using a cell line that could be used for high-throughput screening, the studies were also performed using PMA-differentiated THP-1 cells (Figure 10). The results were identical with the exception that the functionalized MWCNT produced a higher background response, probably due to the PMA activation of the cell. Nevertheless, the raw and pure MWCNT were significantly more toxic and produced significantly more IL-1β and IL-18 compared to the functionalized –COOH MWCNT particles. This clearly demonstrates that the differentiated THP-1 model is a potentially important model for accessing the biological activity of nanomaterials. It has the advantages of generating large cell numbers necessary for a high-throughput assay in addition to the fact that it is a human model system.

Discussion

As a class of nanoparticles, MWCNT have been shown to cause cytotoxicity *in vitro* (Hamilton et al., 2007, 2012a,b; Lam et al., 2006; Patlolla et al., 2010) and granulomas and fibrosis *in vivo* using rodent models (Donaldson et al., 2006; Mercer et al., 2010, 2011; Porter et al., 2010, 2012). However, the mechanisms and physical properties accounting for their bioactivity remain uncertain. In order to address these questions, utilizing purified samples and derivatives can help understanding the role that physical properties of MWCNT play in the bioactivity of nanomaterials. The purpose of this study was to determine the effects of purification and –COOH functionalization on the bioactivity of MWCNT. In addition, since the NLRP3 inflammasome plays an important role in the bioactivity of an increasing number of particles that have now been associated with ''sterile inflammation'', *in vitro* inflammasome activation in addition to toxicity of the modified MWCNT were examined. Furthermore, the bioactivity of the –COOH functionalized MWCNT were tested *in vivo* using C57Bl/6 mice, which are described in a separate manuscript (Sager et al., 2013).

In vitro toxicity and NLRP3 inflammasome activity results indicated the same relational pattern among the four MWCNT examined in this study. The raw MWCNT were the most bioactive followed by the purified, that were much more active than the ''raw'' functionalized, followed by the purified and functionalized being the least active. The results showing that the purified MWCNT had less bioactivity than the ''raw'' material is consistent with the previously reported role of metals and in particular Ni on single-walled carbon nanotubes (Liu et al., 2007, 2008), MWCNT (Hamilton et al., 2012a, b) bioactivity, and a report of soluble Ni activating the NLRP3 inflammasome (Pietruska et al., 2011). Although purification of MWCNT had minimal effects on toxicity, the effects on NLRP3 inflammasome activity were significantly different. Characterization of the purified MWCNT demonstrated that not only was the amorphous carbon layer removed, but also the Ni content was decreased by 60%.

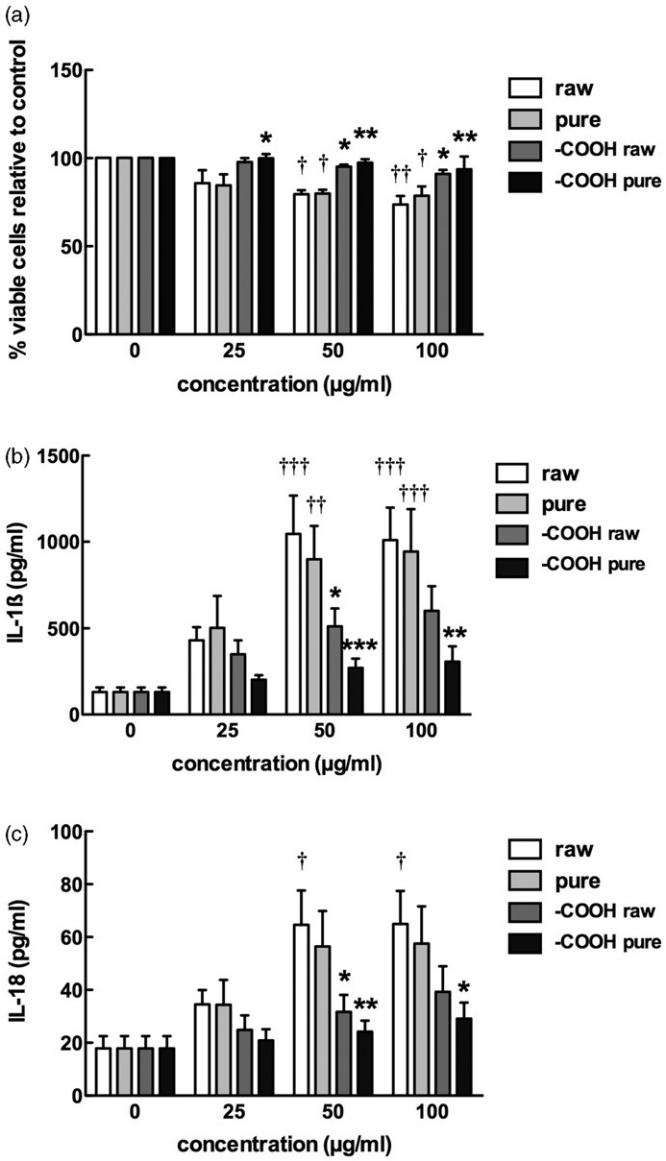

Figure 10. Supportive experimental data obtained in the transformed human THP-1 cell line exposed to MWCNT for 24 h. The results are completely consistent with those found in the mouse AM cell shown in Figure 7; (a) cell viability by MTS assay expressed as mean ± SEM percent relative to unstimulated control cultures, (b) IL-1β production expressed as mean ± SEM, (c) IL-18 production expressed as mean ± SEM. Asterisks indicate $*p<0.05$, $**p<0.01$, or $***p<0.001$ by Bonferroni's correction following two-way ANOVA compared to ''raw'' at each corresponding concentration. Daggers (†) indicate comparison to the 0 μg/ml or baseline condition, with the number indicating the significance level similar to the asterisks. Sample $n=3$.

Although it cannot be determined for certain that the removal of the Ni was solely responsible for the decreased bioactivity of the purified MWCNT, the results are consistent with that notion, since amorphous carbon by itself has not been reported to cause toxicity or cause NLRP3 inflammasome activation.

Functionalization of the MWCNT with –COOH had dramatic effects on both the properties and bioactivity of the MWCNT. Raw or purified MWCNT resuspend very poorly and form large agglomerates even when using protein/lipid dispersants. Therefore, the bioactivity is most likely due to these agglomerates being taken up by macrophages rather than any single MWCNT. In contrast, the functionalized MWCNT were well dispersed in water and formed stable suspensions. Furthermore, functionalization of the MWCNT dramatically decreased bioactivity (toxicity and activation of the NLRP3 inflammasome). The mechanism for the decrease in bioactivity could be due to the changes in surface properties, better dispersion, and/or differences in the extent of phagocytosis or mechanism of phagocytosis. Clearly, the changes in surface properties (hydrophobic to hydrophilic) had a significant impact on dispersion status. However, macrophages appear to take up both the un-functionalized and functionalized MWCNT (Figure 8). From these studies, quantitation of the uptake was not practical, but it did appear that there was a difference in compartmentalization of the internalized MWCNT. The fact that the functionalized MWCNT maintain a stable suspension could potentially affect the amount of material that comes in contact with an adherent cell. However, Figure 9 shows that despite this limitation, more fuctionalized MWCNT get in to the AM than the raw material at 3 to 4 h. Figure 7 suggests the non-functionalized MWCNT were present in large phago-lysosomes, while functionalized MWCNT appear to be in much smaller phago-lysosomes, but were also present in the cytoplasm early following exposure. Therefore, the pathways for internalization may be different for the two types of MWCNT to account for this difference in distribution. Since both types of MWCNT were taken up by macrophages it would argue that simply taking up the MWCNT was not responsible for either toxicity or NLRP3 inflammasome activation.

These *in vitro* studies support the notion, similar to previous results with TiO_2 nanobelts, that MWCNT activate the NLRP3 inflammasome through a process involving phago-lysosomal lysis since the cathepsin B (CA-074-me) and Caspase-1 (Ac-Try-Val-Ala-Asp-CMK) inhibitors effectively blocked IL-1β production in Figure 6 (Hamilton et al., 2009). Whether any relationship exists between cytotoxicity and inflammasome activation is not clear. Although subtle, the data suggest that cytotoxicity and NLRP3 inflammasome activation appear unrelated (Figure 6). Studies conducted using THP-1 cells also support the notion that the two outcomes are unrelated (Figure 10). These results confirm the relative order of potency of the purified and modified MWCNT and support the notion that differentiated THP-1 cells may be a useful model to study nanomaterial effects on primary macrophages.

The effects of two of the nanomaterials used in this study (purified and functionalized) were compared *in vivo* (Sager et al., 2013). The *in vivo* findings were consistent with these *in vitro* studies since the functionalized were less bioactive than the purified MWCNT. Therefore, the *in vitro* studies were predictive of the *in vivo* outcomes and the results with the THP-1 cells were also predictive of the *in vivo* outcomes. Although many questions remain in the field of nanomaterial toxicology, the results from these studies suggest that *in vitro* studies can be useful in helping to predict *in vivo* outcomes. Furthermore, these studies with MWCNT are consistent with the reports using environmental particulates silica and asbestos (Donaldson et al., 2010; Dostert et al., 2008; Palomaki et al., 2011) and an endogenous crystal uric acid (Dostert et al., 2008), which determined NLRP3 inflammasome activation was important in mediating inflammation

in vivo. Therefore, *in vitro* screening for NLRP3 inflammasome activation should be considered when evaluating potential harmful effects of new nanomaterials.

Acknowledgements

The authors thank Dr. Jim Driver at the University of Montana Electron Microscopy Facility (Division of Biological Sciences) for the EM images of the AM cells and Pam Shaw at the University of Montana Fluorescence Cytometry Core for the Caspase-1 imaging and quantitation.

Declaration of interest

The authors report no conflicts of interest. The production, characterization, and toxicology studies were primarily supported by a NIH grant (1RC2ES018742). The authors acknowledge the following grants that contributed support: NIH R01 ES015497, NSF CBET-0834233, and COBRE P20 RR017670. The facilities and resources used in this work were partially supported by the NSF grant (EPS 0554328 and EPS 1003907) with matching funds from the West Virginia University Research Corporation and the West Virginia EPSCoR Office. The findings and conclusions in this report are those of the authors and do not necessarily represent the views of the National Institute for Occupational Safety and Health.

References

Arend WP, Palmer G, Gabay C. (2008). IL-1, IL-18, and IL-33 families of cytokines. Immunol Rev 223:20–38.

Brozena AH, Moskowitz J, Shao B, et al. (2010). Outer wall selectively oxidized, water-soluble double-walled carbon nanotubes. J Am Chem Soc 132:3932–8.

Buford MC, Hamilton Jr RF, Holian A. (2007). A comparison of dispersing media for various engineered carbon nanoparticles. Part Fibre Toxicol 4:6.

Cassel SL, Joly S, Sutterwala FS. (2009). The NLRP3 inflammasome: a sensor of immune danger signals. Semin Immunol 21:194–8.

Datsyuk V, Kalyva M, Papagelis K, et al. (2008). Chemical oxidation of multiwalled carbon nanotubes. Carbon 46:833–40.

Donaldson K, Aitken R, Tran L, et al. (2006). Carbon nanotubes: a review of their properties in relation to pulmonary toxicology and workplace safety. Toxicol Sci 92:5–22.

Donaldson K, Murphy FA, Duffin R, Poland CA. (2010). Asbestos, carbon nanotubes and the pleural mesothelium: a review of the hypothesis regarding the role of long fibre retention in the parietal pleura, inflammation and mesothelioma. Part Fibre Toxicol 7:5.

Dostert C, Petrilli V, Van Bruggen R, et al. (2008). Innate immune activation through Nalp3 inflammasome sensing of asbestos and silica. Science 320:674–7.

Drenth JP, van der Meer JW. (2006). The inflammasome – a linebacker of innate defense. N Engl J Med 355:730–2.

Feng X, Irle S, Witek H, et al. (2005). Sensitivity of ammonia interaction with single-walled carbon nanotube bundles to the presence of defect sites and functionalities. J Am Chem Soc 127:10533–8.

Ferrari AC, Meyer JC, Scardaci V, et al. (2006). Raman spectrum of graphene and graphene layers. Phys Rev Lett 97:187401.

Forrest GA, Alexander AJ. (2007). A model for the dependence of carbon nanotube length on acid oxidation time. J Phys Chem 111: 10792–8.

Hamilton RF, Buford M, Xiang C, et al. (2012a). NLRP3 inflammasome activation and related lung pathology is associated with MWCNT nickel contamination. Inhal Toxicol 24:995–1008.

Hamilton RF, Buford MC, Wood MB, et al. (2007). Engineered carbon nanoparticles alter macrophage immune function and initiate airway hyper-responsiveness in the BALB/C mouse model. Nanotoxicology 1:104–17.

Hamilton RF, Girtsman TA, Xiang C, et al. (2012b). Nickel contamination on MWCNT is related to particle bioactivity but not toxicity in the THP-1 transformed macrophage model. Int J Biomed Nanosci Nanotechnol (accepted for publication).

Hamilton Jr RF, Thakur SA, Mayfair JK, Holian A. (2006). MARCO mediates silica uptake and toxicity in alveolar macrophages from C57BL/6 mice. J Biol Chem 281:34218–26.

Hamilton RF, Wu N, Porter D, et al. (2009). Particle length-dependent titanium dioxide nanomaterials toxicity and bioactivity. Part Fibre Toxicol 6:35.

Hudson JL, Casavant MJ, Tour JM. (2004). Water-soluble, exfoliated, nonroping single-wall carbon nanotubes. J Am Chem Soc 126: 11158–9.

Jain S, Thakare VS, Das M, et al. (2011). Toxicity of multiwalled carbon nanotubes with end defects critically depends on their functionalization density. Chem Res Toxicol 24:2028–39.

Jozefowski S, Sulahian TH, Arredouani M, Kobzik L. (2006). Role of scavenger receptor marco in macrophage responses to CpG oligodeoxynucleotides. J Leukoc Biol, 80:870–9.

Lam CW, James JT, Mccluskey R, et al. (2006). A review of carbon nanotube toxicity and assessment of potential occupational and environmental health risks. Crit Rev Toxicol 36: 189–217.

Li MZ, Wu N, Mao SX. (2002). Length-scale-controlled interfacial toughening and weakening in metal/ceramic layered materials. Philos Mag A 82:1049–71.

Lim MS, Feng K, Chen XQ, et al. (2007). Adsorption and desorption of stearic acid self-assembled monolayers on aluminum oxide. Langmuir 23:2444–52.

Liu X, Guo L, Morris D, et al. (2008). Targeted removal of bioavailable metal as a detoxification strategy for carbon nanotubes. Carbon 46: 489–500.

Liu XY, Gurel V, Morris D, et al. (2007). Bioavailability of nickel in single-wall carbon nanotubes. Adv Mater 19:2790–6.

Long B, Wu TM, Stellacci F. (2008). Ultra-fast and scalable sidewall functionalisation of single-walled carbon nanotubes with carboxylic acid. Chem Commun (Camb) 2788–90.

Martinon F, Mayor A, Tschopp J. (2009). The inflammasomes: guardians of the body. Annu Rev Immunol 27:229–65.

Mercer RR, Hubbs AF, Scabilloni JF, et al. (2010). Distribution and persistence of pleural penetrations by multi-walled carbon nanotubes. Part Fibre Toxicol 7:28.

Mercer RR, Hubbs AF, Scabilloni JF, et al. (2011). Pulmonary fibrotic response to aspiration of multi-walled carbon nanotubes. Part Fibre Toxicol 8:21.

Palomaki J, Valimaki E, Sund J, et al. (2011). Long, needle-like carbon nanotubes and asbestos activate the NLRP3 inflammasome through a similar mechanism. ACS Nano 5:6861–70.

Patlolla A, Knighten B, Tchounwou P. (2010). Multi-walled carbon nanotubes induce cytotoxicity, genotoxicity and apoptosis in normal human dermal fibroblast cells. Ethn Dis 20: S165–72.

Peng H, Alemany LB, Margrave JL, Khabashesku VN. (2003). Sidewall carboxylic acid functionalization of single-walled carbon nanotubes. J Am Chem Soc 125:15174–82.

Pietruska JR, Liu X, Smith A, et al. (2011). Bioavailability, intracellular mobilization of nickel, and HIF-1α activation in human lung epithelial cells exposed to metallic nickel and nickel oxide nanoparticles. Toxicol Sci 124:138–48.

Porter DW, Hubbs A, Chen BT, et al. (2012). Acute pulmonary dose-responses to inhaled multi-walled carbon nanotubes. Nanotoxicology. DOI:10.3109/17435390.2012.719649.

Porter DW, Hubbs AF, Mercer RR, et al. (2010). Mouse pulmonary dose- and time course-responses induced by exposure to multi-walled carbon nanotubes. Toxicology 269:136–47.

Pumera M. (2007). Carbon nanotubes contain residual metal catalyst nanoparticles even after washing with nitric acid at elevated temperature because these metal nanoparticles are sheathed by several graphene sheets. Langmuir 23:6453–8.

Ramanathan T, Fisher FT, Ruoff RS, Brinson LC. (2005). Amino-functionalized carbon nanotubes for binding to polymers and biological systems. Chem Mater 17:1290–5.

Sager TM, Wolfarth MW, Andrew M, et al. (2013). Effect of multi-walled carbon nanotube surface modification on bioactivity in the C57Bl/6 mouse model. Nanotoxicology (in press).

Shao L, Tobias G, Salzmann CG, et al. (2007). Removal of amorphous carbon for the efficient sidewall functionalisation of single-walled carbon nanotubes. Chem Commun (Camb) 5090–2.

Tafen DN, Wang J, Wu NQ, Lewis JP. (2009). Visible light photocatalytic activity in nitrogen-doped TiO_2 nanobelts. Appl Phys Lett 94: 093101-1–3.

Tan GL, Hommerich U, Temple D, et al. (2003). Synthesis and optical characterization of CdTe nanocrystals prepared by ball milling process. Scripta Mater 48:1469–74.

Tschopp J, Schroder K. (2010). NLRP3 inflammasome activation: the convergence of multiple signalling pathways on ROS production? Nat Rev Immunol 10:210–15.

Wang L, Mercer RR, Rojanasakul Y, et al. (2010). Direct fibrogenic effects of dispersed single-walled carbon nanotubes on human lung fibroblasts. J Toxicol Environ Health A 73:410–22.

Wang Y Iqbal Z, Mitra S. (2006). Rapidly functionalized, water-dispersed carbon nanotubes at high concentration. J Am Chem Soc 128:95–9.

Wang ZW, Shirley MD, Meikle ST, et al. (2009). The surface acidity of acid oxidised multi-walled carbon nanotubes and the influence of in-situ generated fulvic acids on their stability in aqueous dispersions. Carbon 47:73–9.

Worsley KA, Kalinina I, Bekyarova E, Haddon RC. (2009). Functionalization and dissolution of nitric acid treated single-walled carbon nanotubes. J Am Chem Soc 131:18153–8.

Wu NQ, Fu L, Su M, et al. (2004). Interaction of fatty acid monolayers with cobalt nanoparticles. Nano Lett 4:383–6.

Wu NQ, Wang J, Tafen D, et al. (2010). Shape-enhanced photocatalytic activity of single-crystalline anatase TiO_2 (101) nanobelts. J Am Chem Soc 132:6679–85.

Yazdi AS, Guarda G, Riteau N, et al. (2010). Nanoparticles activate the NLR pyrin domain containing 3 (NLRP3) inflammasome and cause pulmonary inflammation through release of IL-1alpha and IL-1beta. Proc Natl Acad Sci USA 107:1944–54.

Zhang QA, Sun T, Cao F, et al. (2010). Tuning the shape and thermoelectric property of PbTe nanocrystals by bismuth doping. Nanoscale 2:1256–9.

Zhi MJ, Mariani N, Gemmen R, et al. (2011). Nanofiber scaffold for cathode of solid oxide fuel cell. Ener Environ Sci 4:417–20.

Zimmerman JL, Bradley RK, Huffman CB, et al. (2000). Gas-phase purification of single-wall carbon nanotubes. Chem Mater 12: 1361–6.